Journal of Materials Chemistry C

Accepted Manuscript

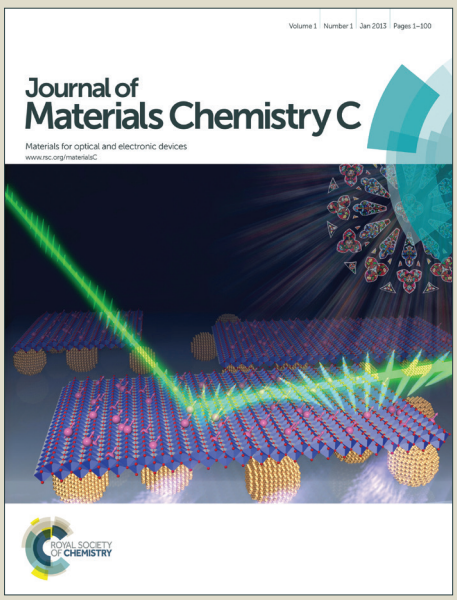

ROYAL SOCIETY OF CHEMISTRY

www.rsc.org/materialsC

Journal Name

RSCPublishing

ARTICLE

Hydrogen-Bonded Supercoil Self-Assembly from Achiral Molecular Components with Light-Driven Supramolecular Chirality

Cite this: DOI: 10.1039/x0xx00000x

Received 00th January 2012,
Accepted 00th January 2012

DOI: 10.1039/x0xx00000x

www.rsc.org/

Yangyang Wang,[ab] Deyan Zhou,[a] Haining Li,[a] Ruiru Li,[a] Yueyao Zhong,[ab] Xuan Sun,*[a] Xun Sun[b]

Supercoils self-assembled from achiral molecular two-components have been synthesized in order to better understand the structure and functionality of this chiral supramolecular association. The two-component synthon is a complementary hydrogen-bond pair having one melamine core and three photoaddressable azobenzene units, which self-assembled into long and helical fibers with intrinsic conformational chirality. Hierarchical self-assembly was presented where one-dimensional helixes bundled into a higher order optically active supercoil structure, leading to spontaneous chiral symmetry breaking and amplification of chirality. Circular dichroism (CD) spectroscopy, transmission electron microscopy (TEM) and atomic force microscopy (AFM), as well as X-ray diffraction (XRD) techniques reveal the chiral nature of the assembly. Accordingly, a plausible mechanism of a hierarchical self-assemble process has been proposed, which presents a valid approach for constructing supramolecular chirality from achiral molecular building blocks through non-covalent interactions. The morphology and chirality of the supercoils demonstrate photoresponsbility, which is induced from the photoisomerization of the azobenzene components within the self-assembled nanostructures. Furthermore, the supercoil is highly proton-conductive material because of its highly ordered structure and the proton transfer between the H-bonded melamine and azobenzene units within this two-component association.

1. Introduction

Supramolecular chirality involves the nonsymmetrical arrangement of molecular components in noncovalent assemblies.[1] Artificial systems with supramolecular chirality have been greatly developed in the last decade to understand the origin of homochirality in nature, and to mimic biological functions as well.[1-3] To control the supramolecular chirality, the general method is the introduction of chiral centers in the building blocks, namely the asymmetric induction, to achieve the chiral amplification.[1] While symmetric breaking is rarely observed in homogeneous systems that are racemic or achiral. Achiral building blocks, either intrinsically achiral molecules or a racemate, are found to occasionally self-assemble into chiral nanostructures, which are crucial for revealing the chirality arising and transferring from the molecular to the supramolecular, and to the periodic or quasiperiodic array levels.[4,5,6a] Kimuraet al. reported the first example of the helical nanoscopic fibers achieved from achiral disk-like molecules with triphenylene cores.[7] Hierarchical self-assembly process, namely bundling of the twisted nanofibers was presented therein, but was never investigated intensively. Recently, Meijer and co-workers gave the first in-depth report on symmetry-breaking in a two-step self-assembling system, relying on a hierarchical self-assembly process of a class of achiral, partially fluorinatedbenzene-1,3,5-tricarboxamides.[4b] It was revealed that the weak interactions between fluorine atoms and electron-deficient (CF_2-H) hydrogen atoms on the periphery of the one-dimensional helical stacks is a crucial element in the symmetry breaking in bundling of the one-dimensional aggregates. However, the self-assembling and the functions of the helices (developed from the achiral molecules) are far from being investigated.

Subunits with C_3 rotational symmetries (or un-symmetric) were found highly attractive to construct helical one-dimensional supramolecular aggregates relying on intermolecular threefold H-bonding in combination with π-π stacking.[8] Melamine, a typical C_3-symmetric molecule, has

demonstrated an outstanding supramolecular synthon for construction of 3D structure.[9a,10] While fabrication of supramolecular helical structure using melamine as building blocks was investigated relatively rare. Nandi etc. reported a riboflavine(R)–melamine(M) hydrogel system, of which the morphology was tuned from helical fiber to rod-like to tubular structure by changing the composition of the RM components.[11a] Melamine can provided as the central part of a disk-like structure that can stack orderly and offers the possibility of hydrogen-bond interaction with acids. Sierra and the co-workers have designed several systems in which the melamine-derived core interacted with the V-shaped acids to construct the well-defined columnar mesophases.[12] It was proposed that the compact columnar packing was formed by synergistic π-stacking of the melamine core and the paralleling of the peripheral long-arms of the V-shaped molecules. To favor this arrangement, a disposition of propeller-like conformation is preferred, which induced a helical arrangement within the column. However, only by introduction of the chiral building blocks and/or by circularly polarized light (CPL), could the optical activity be induced and controlled for the above helical columnar mesomorphic systems. Moreover, it was pointed out that when the V-shaped acids with short arms, such as 3,5-bis(4-decyloxybenzoyloxy)benzoic acid and 3,5-bis-(3,4,5-tridecyloxybenzoyloxy)benzoic acid were used, mesomorphic columnar structure could not be obtained, indicating of the crucial role of the molecular structure for the helical arrangement formation.[12a] Other than the V-shaped or banana-like molecules that have large steric effect, will the helical stacking be kept when a small molecule with more "straight" structure is applied instead? If then, by design of the building blocks, high level of control can be achieved to facilitate a precise incorporation of functional groups in various parts of the helix. Herein we report the formation of mesoscopic supercoil structure from the co-assembly of a pair of achiral triply hydrogen-bonded complementary components, carboxylic acid substituted azobenzene (**A** in Figure 1) and melamine (**M**). Symmetry-breaking is observed in this self-assembling system, which is made up from achiral components with quite simple molecular structure. This is extremely helpful for in-depth insight into the amplification of chirality processes, such as the origin of the CD effects and the importance of hydrogen-bonding interactions during the aggregation process.

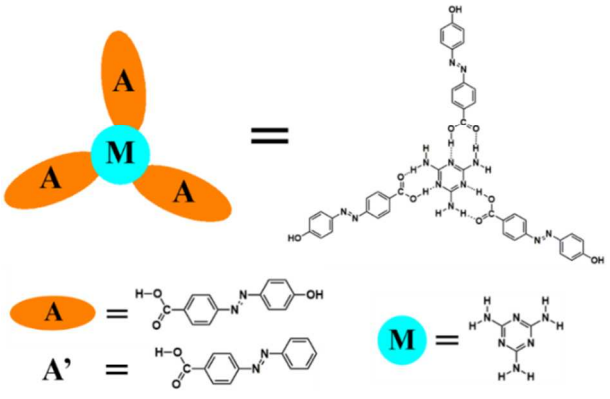

Figure 1. Chemical structures of **A**, **M** and **A'**, and the schematic representation of the **M•A$_3$** complex (the orange parts represent the molecule **A**, and the blue part represents the molecule **M**).

Moreover, The photoisomerization property of the present azobenzene units favor the supercoils with photoresponsibility, the morphology and CD activity of the multi-component assembling systems can therefore readily be tuned by external light-stimuli, which demonstrate great potential for construction of smart supramolecular materials with switchable properties.[6,13,14] In addition, the proton-conductive characteristics of the supercoils are examined, considering the highly ordered structure of the supercoils and the proton transfer between the two components **A** and **M**. It shows the typical electrolyte conductive property, indicating the supercoils to be good proton conductive material as potential fuel cells. The system studied herein provides a model for construction of functional chiral supramolecular structure via appropriate tailoring with the achiral functional groups.

2. Experimental

Instruments and measurements

^{1}H NMR spectra were recorded on a Bruker DPX 300 spectrometer (300 MHz) using SiO_2 as an internal reference. Matrix-assisted laser desorption/ionization time-of-flight (MALDI-TOF) mass spectra were detected on a Bruker BIFLEXIII ultrahigh-resolution. Elemental analysis was conducted on Vario EL CUBE. Thermogravimetric analysis was detected on Simultaneous Thermal Analyzer. Absorption spectra were measured on a Hitachi U-4100 spectrophotometer. CD spectra were measured on a Jasco J-810 circular dichroism spectropolarimeter in quartzcells with a thickness of 1 mm. FT-IR measurements were recorded for KBr pellets with a resolution of 2 cm^{-1} using aVER-TEX-70 (Bruker) spectrometer. A CHF-XM35-500W ultrahigh pressure short arc mercury lamp was used to carry out the photoisomerisation using optical filters with wavelength of 365 nm for *trans*-to-*cis*, and >400 nm for *cis*-to-*trans* reactions. Transmission electron microscopy (TEM) images were recorded on a JEOL-100CX II electron microscope operated at 100 kV. A high-resolution transmission electron microscopy (HR-TEM) measurement was performed with a JEOL-2010 working at 200 kV. For TEM and HR-TEM imaging, a drop of sample solution was cast onto a copper grids prayed with carbon. The powder X-ray diffraction (XRD) patterns were recorded using a Rigaku D/Max 2200-PC diffractometer with Cu-Ka radiation (λ = 0.15418 nm) and agraphite monochromator at ambient temperature. All calculations were carried out using the density functional theory (DFT) method at the b3lyp/6-311+g** level. All of the calculations were performed using the Gaussian 09 program at the Shandong Province High Performance Computing Centre.

Materials and methods

Unless stated otherwise, all reagents and anhydrous solvents were purchased from commercial suppliers and used without further purification.

Synthesis of 4-hydroxy-4'-carboxyl azobenzene (A). 4-Aminophenol (5 g, 0.046 mol) was added to the hydrochloric acid solution (20%, 23 ml), which was stirred until dissolved. The water solution (15 ml) of sodium nitrite (3.3 g, 0.0478 mol) was added dropwisely to the above solution within 1 h and then stirred for another 30 minutes. The temperature of the whole process was kept at 2 °C. Phenol (4.35 g, 0.0463 mol) and sodium hydroxide (1.85 g, 0.0463 mol) were dissolved in water (50 ml), and added dropwisely to the above diazonium salt solution within 1 h, keeping the temperature under 2 °C. The

reaction was completed after stirring for another 3 h at 2 °C. After stewing at room temperature for 24 h, orange product was precipitated, and was chromatographed on silica gel using ethyl acetate and petroleum ether (v/v = 1/2) as eluent. The second fraction was collected and evaporated, giving orange solid (9.11g) with yield of 81.8%. ^{1}H NMR (Acetone, 300 MHz), δ (ppm): 13.03 (s, 1 H, COOH), 10.518 (s, 1 H, OH), 8.12-8.09 (t, 2 H, *Ar*), 7.89-7.83 (m 4 H *Ar*), 6.98-6.95 (m 2 H *Ar*), MS: m/z 241.2366 $[M-H]^+$.

Synthesis of 4-carboxyl azobenzene (A'). Compound **A'** was synthesized according to the procedure reported previously.[15] Red solid (7.01 g) was obtained with yield of 85.8%. ^{1}H NMR (Acetone, 300 MHz), δ (ppm): 8.27-8.22 (d, 2 H, *Ar*), 8.03-7.97 (m, 4 H, *Ar*), 7.65-7.59 (m, 3H, *Ar*), MS: m/z225.0645 $[M-H]^+$.

Fabrication of the supramolecular self-assembly. Hydrogen-bonded supramolecular structures were prepared by mixing of **A** (or **A'**) with M at room temperature at a molar ratio of 3:1. A (or **A'**) was completely dissolved in THF (5.76 mg cm^{-3}) and drop on the aqueous solution of M (1.0 mg cm^{-3}) with a volume ratio of 1:1. Along with the permeation and volatilization of THF, orange-red colored aggregates forms gradually at the interface and precipitated finally.

Device fabrication

Au electrodes were thermally evaporated onto the SiO_2/Si substrate by using a shadow mask. This interdigitated array electrode is composed of 6 pairs of electrode digits (n). The interelectrode spacing (d) is 0.24 mm, the overlapping length of the electrodes of (L) is 2.6 mm, and the calculated thickness of the aggregates (h) is about 20 nm. The aggregates obtained from the above fabrication method were cast onto the substrate uniformly. The current–voltage characteristics were obtained with a Keithley 4200 semiconductor characterization system at room temperature in air. Current–voltage (*I–V*) curves were registered in the -10 to 10 V voltage range with 1 V increments. Conductivity, σ, can be calculated by the following equation.[16]

$$\sigma = \frac{dI}{(2n-1)LhV}$$

3. Results and discussion

Self-assembly in solution

When THF solution of **A** and aqueous solution of **M** mixed together, orange-red aggregates formed gradually at the interface and precipitated along with evaporation of the THF. The self-assemble process and the interaction between **A** and **M** were monitored by UV/Vis and fluorescence spectroscopy. As shown in Figure 2a, the aggregate **A-M** suspension in water shows a strong absorption at 353 nm, which is slightly blue-shifted and a small decrease in the intensity compared with the highly dispersed THF solution of **A**. According to the molecular exciton theory,[17] this excitonic effect is pointed to the interchromophore interactions between the **A** chromophores within the dimer,[18] which is indicative of the excitonically coupled aggregates in water.

In contrast to the UV/Vis spectra, the fluorescence spectra exhibited greater difference between the **A-M** aggregate and that of the **A** monomer (Figure S1). When excited with 320 nm, compound **A** exhibits a weak emission centered at 405 nm, while the **A-M** aggregate shows a broad emission band with a embossment at 468 nm, and the intensity of the emission drastically decreased. This broad emission is unanimously designated to the excimer formation, indicating the strong π-π interaction between the two stacked **A** molecules, confirming the H-type aggregation.

THF solution of **A** and aqueous solution of **M** were circular-dichroism (CD) inactive, as expected for achiral molecules. Intriguingly, the CD spectra of the aggregation (Figure 2b) shows significant Cotton effect at 316 nm, which is in agreement with the absorption spectrum. In view of the achiral two molecules **A** and **M**, the CD signals clearly indicate the chiral symmetry breaking occurs in the **A-M** assembly, which should be induced from a helical disposition of at least two chromophores **A**.[18] The aggregation of **A-M** had the same CD spectrum after being stored for several months, thus the racemization did not occur after the helical stacks had formed. In general, the CD effects show a negative sign. Further repeating experiments revealed that positive CD effects were rarely observed. This is a remarkable observation since a stochastic process in the absence of chiral information should result in an equal occurrence of positive and negative CD effects. It is suggested that surface-assisted secondary nucleation may occur during the self-assembly process, which is responsible for the supramolecular chiral symmetry breaking.[4b]

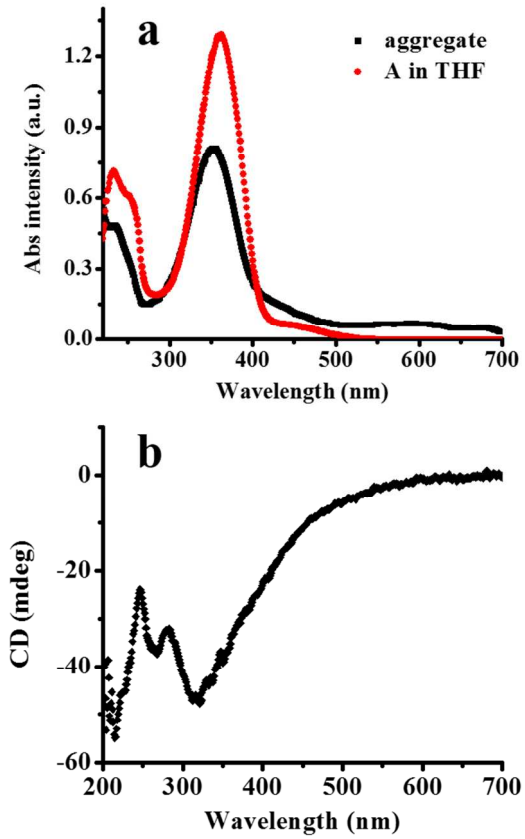

Figure 2. (a) UV-vis spectra of the self-assembled suspensions in water and the highly dispersed molecule **A** in THF at c = 2.5×10^{-5} mol L^{-1}, respectively. (b) CD measurements of the self-assembled suspension in water.

Self-assembly in bulk

From the above spectroscopic probing, it can be deduced that **A** and **M** associate together to form a certain chiral supramolecular structure. Since both the two component **A** and **M** are achiral, evidently the only possibility for the origin of the chirality is that **A** and **M** associate together to form an intrinsic propeller-like conformational chirality. According to arguments on assembling behavior of the C_3 symmetry molecules, such as the melamine derivatives,[11,12] **A** and **M** here as a pair of hydrogen-bonded complementary components, are inclined to be associate by threefold H-bonding, leading to the construction of well-defined organized structures as shown in Figure 1. Significant changes in the infrared spectra (Figure S2) of the association **A**-**M** from its separate components clear indicate the H-bonding between **A** and **M**. In the 3000~3600 cm^{-1} region, the stretching vibration of N–H at 3463, 3416 and 3337 cm^{-1} in non-associated **M** vanished upon complexation, indicating presence of H-bonding interaction between **A** and **M**.[11b] Marked difference is also observed between the acid **A** and the association **A**-**M**. In acid **A**, C=O stretching band appears at 1668 cm^{-1}, corresponding to the cyclic dimeric form. Upon association with **M**, a broad band appeared at around 1680 cm^{-1}. This high energy shift may be attributed to the H-bonding between -NH_2 group of **M** with C=O groups of A.[11b] Both the separate components and the association **A**-**M** show several bands corresponding to N–H and O–H bonds that are associated and non-associated through H-bonds.

According to TGA and elemental analysis (Figure S3, Table S1), **A** and **M** associate into **M•A$_3$** complex within the aggregates, which is also confirmed by ^{1}H NMR study. The ^{1}H NMR spectrum of complex **M•A$_3$** is shown in Figure S4, along with those of the separate components. All six N–H protons of the non-associated **M** appeared as a sharp single peak at 5.984 ppm. The non-associated **A** demonstrated several doublet-peaks between 6.9 and 8.1 ppm, corresponding to the protons on the benzene rings of **A**. Protons corresponding to –OH and –COOH appears as two weak broad signals in the downfield region at around 10.5 and 13.0 ppm, respectively. Upon complexation, all the signals of the protons on the benzene rings of **A** shifted a little with several splitting peaks appeared. The signal of the –OH shifted upfield to 9.78 ppm. The most remarkable change observed in the ^{1}H NMR spectrum of complex **M•A$_3$** is that, the signal of the proton on the –COOH groups disappeared; meanwhile, a broad signal corresponding to the resonance of the –NH of the triazine appeared at around 3.45 ppm. These significant changes explicitly demonstrate the hydrogen-bonding formation and the proton transfer between the **A** and **M** molecules. Specifically, the ratio of the protons coming from **A** and **M**, respectively, is 3:1 in the associated complex, which is unambiguously indicative of the presence of a supramolecular complex **M•A$_3$**.

Transmission electron micrograph (TEM) image revealed the long twisted fibers at the macroscopic level, which are approximately 260 nm wide and 30-40 micrometers long with a helical pitch of approximately 1700 nm (Figure 3a, b). These results, in combination with CD effects, confirm the chiral nature of the **M•A$_3$** complexation. Although twisted fibers have been observed in many supramolecular assemblies of molecular components bearing chiral substituents, the formation of twisted fibers from achiral molecular components is rare. The observed widths of the fibers are significantly wider than the estimated diameter of **M•A$_3$** (about 3.3 nm estimated from the computer-simulated molecular model), suggesting that the fibrous structure may be composed of bundles of one-dimensional stacks of **M•A$_3$**. Careful analyses of the TEM images showed that these twisted fibers are indeed formed by right- and left-handed helical ribbons twined together. The bundling of the single-handedness ribbons clearly indicates a hierarchical self-assembling process, where surface-assisted secondary nucleation takes place as deduced from the CD signals.

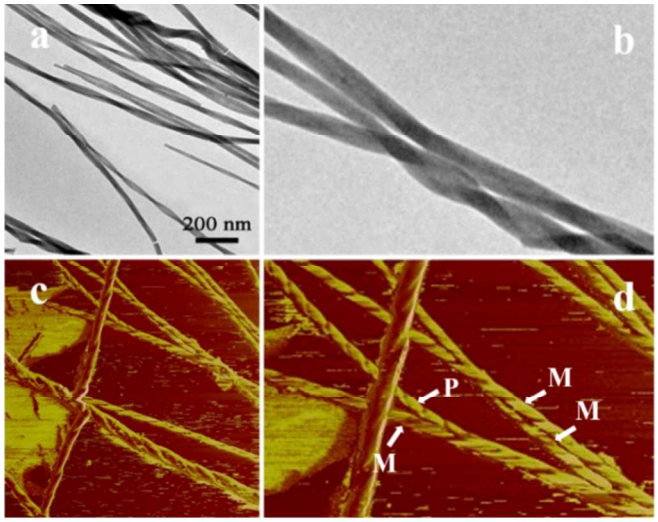

Figure 3. (a), (b) TEM and (c), (d) AFM observation of the self-assembled helixes andsupercoils with labeled handedness.

Details of the fibers formed by **M•A$_3$** is further investigated with atomic force microscopy (AFM) measurement (Figure 3c, d). AFM shows a larger area with many supercoils in close proximity to one another, demonstrating a hierarchical self-assembly of the complex **M•A$_3$**. At the very beginning, **M•A$_3$** stacks into one-dimensional helical ribbon with single-handedness and shorter helical pitch (~ 200 nm). The handedness of the initiating ribbon is randomly dominated, because of the achiral nature of the unit molecule. Then, the helical ribbons with opposite handedness bundle together to form supercoils with larger helical pitch as also observed in TEM image. It is noted that, only the helixes with opposite handedness, namely the right-handed (*P*) and left-handed (*M*), can coupled intensively to form the supercoil with long helical pitch; on the other hand, the helixes with the same handedness will not interact with each other, therefore keeping their original chirality with short helical pitch.[8b] On account of such hierarchical assembly, we can obtain either levo- or dextro-rotatory enantiomers, as is evidenced by the CD curves. This two-step self-assembly behavior involves a kinetically controlled secondary nucleation, in which the one-dimensional helical aggregates bundle into a higher order aggregate, the supercoil.[4b] The –OH groups at the end position of the molecule **A** is expected to be essential for the secondary nucleation by dimerization through intermolecular H-bonds.[19] As for verification, the azobenzene analogue **A'** (Figure 1) was synthesized and the corresponding assembly **M-A'** was prepared for comparison. Amorphous film was obtained which showed silent CD signal. The differences of the self-assemble behavior between **A** and **A'** indicate the significance of the –OH end groups in the supercoil formation. Hence, we propose that multiple –OH groups are decorated on the periphery of the one-dimensional **M•A$_3$** aggregates to form highly polarized chains, leading to tight interaction between two or more **M•A$_3$** stacks, which facilitate the hierarchical bundling or surface-

assisted secondary nucleation of one-dimensional aggregates into optically active supercoils. It is noted that, such hierarchical growth of highly ordered helical materials at mesoscopicscales from the achiral components have rarely been reported so far,[4b] which is fascinating for mimicking the delicate architectures found in nature.[3] This unanticipated supercoil structure was attributed to the helical supramolecular stacking of the C_3 symmetrical **M•A$_3$** association, demonstrating the structural information transformation from the molecules to the supramolecular complexation, and from the supramolecule to the supercoil levels. The internal structure of the supercoils will be discussed in detail in the next section combined with XRD characterization.

X-ray diffraction (XRD) and formation of the supercoils

As shown in Figure 4, strong and successive periodic diffraction peaks are performed in the XRD patterns, which is indicative of the long-range order of the assembly. Small-angle X-ray diffraction (SAXD) patterns revealed the presence of a set of Bragg reflections corresponding to the *d* value at 2.25, 1.13, 0.97, 0.77 and 0.75 nm, which could be indexed most likely with a rectangular pattern as (100), (200), (210), (220), and (300) with lattice parameters of a = 22.5 Å, and b = 19.2 Å. As optimized by using b3lyp/6-311+g** program, the ground-state geometry of **M•A$_3$** in the gas phase presents a windmill structure with diameter of about 3.3 nm, and the three **A** arms prefer the *trans*-conformation with length of about 1.2 nm. The presence of periodic structures with repeated layer spacing of 2.25 nm is indicative of an interdigitation of the neighboring **A** components as illustrated in Figure 4, which is corresponding to strong column-to-column correlations induced mainly from the hydrogen-bonding of the end –OH groups, and is responsible for close packing of the helical columns into supercoils with long helical pitch as demonstrated in AFM.[8b] The WAXD profiles (Figure S5) showed sharp reflections in the 2θ range of 15–35°, which were originated from the typical crystalline arrangement of **M** an **A**, respectively. The broad reflections close to 2θ = 27° in the wide-angle region suggest the one-dimensional stacking of the C_3 symmetrical disk-like molecules **M•A$_3$** in the orthogonal direction of the molecular plane through π-π stacking in combination with interlayer H-bonding. To minimize the steric hindrance between the adjacent **A** arms, stacking along this direction prefer a disposition of propeller-like conformation, resulting in an intrinsic conformational chirality to form the helical one-dimensional aggregation. Then by interdigitation of the highly polarized undulated periphery of helical columns with opposite handedness, columns are coupled strongly. When the columns have the same handedness, symmetry constraints limit the column-to-column correlations. Such a system is indeed supported from the hypochromatic shift in the electronic absorption and the CD signatures. Based on the analysis from spectroscopies and the electron microscope observation, the packing model of the supercoils is proposed and illustrated in Figure 4. The proposed mechanism has the potential to reveal the proton conductivity of the self-assembly that has highly ordered structure relying on intermolecular H-bonding incombination with π-π stacking.

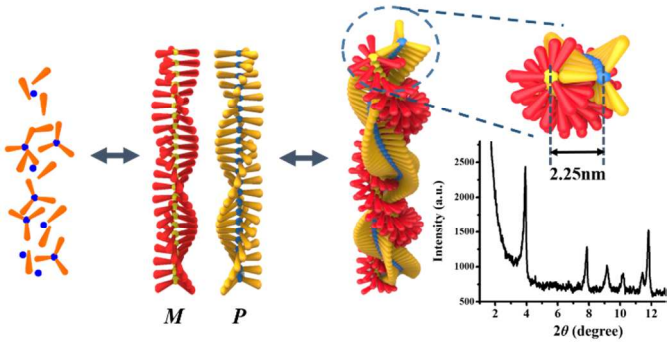

Figure 4. Schematically representation of the supercoil self-assembled from C_3 **M•A$_3$** complex, and the SAXD patterns of the supercoils. 2θ is the diffraction angle. λ = 0.1542 nm (Cu Kα line).

Some further work such as tailoring and decorating on the **A** components maybe needed to gain a detailed understanding of the supramolecular chirality exhibited by the triply H-bonded complementary achiral components; however, we can currently propose that the chirality achieved in the present system originates from the supramolecular organization of the exquisitely designed molecular couples, of which the helical stacking is closely related to the molecular structure of the **A** components, including the rigid plane, the dimension of the molecule and the polar head, etc. If **A** was substituted by benzoic acid or hydroxybenzoic acid to interact with **M** in the same condition, rod-like crystals or straight belt-like structure in micrometer scale were obtained instead. Anyway, the present supramolecular chiral system is particularly interesting, since the presence of multiple molecular-scale species offers the possibility of introducing multifunctionality to these materials.

Photoresponsibility of the supercoils

Stimuli-responsive nano-materials have attracted great attention because of their potential applications in drug or gene delivery purposes and cancer therapy.[9b] Azobenzene, of which the photo-induced E/Z isomerization was well-documented,[20-25] is favorable unit to confer on the system the ability to respond to light as an external stimulus. Indeed, we[6] and many other researchers[26] have demonstrated that the photoisomerization of azobenzene proceeded with a large structural change that affects the dipole moment and geometry at the molecular level, which would trigger great effects at the macroscopic level.

Herein, irradiate the aqueous suspension of the **M•A$_3$** supramolecular aggregates with UV light (365 nm), great changes can be observed as shown in the electronic absorption spectra (Figure S6a). Two stages of change was detected: the intensity of the main absorption band at 350 nm was increased at the beginning, then decreased along with the appearance of a new broad band in the lower energy region (400~500 nm). In the first stage, the absorption enhancement effect may reiterate that the molecules exist in their monomeric form because of the assembly broken under the light irradiation. While the absorption changes in the second stage unambiguously indicative of the *trans*-to-*cis* isomerization of **A**. After illumination for 20 mins, almost no obvious change can be observed, indicating the photostationary state (PSS). Upon irradiation with visible-light (420 nm), the absorption spectra recovered partially, which should be ascribed to the isomerization of the **A** units from the *cis* state to the *trans* state.

Accordingly, the CD spectra (Figure S6b) also demonstrate distinct changes when exposing the supercoils into UV light. The molar magnitude of CD effect (mdeg) decreases along with the irradiation time. Since the CD signal comes from the helical disposition of the molecules within the supracoil, the changes observed in the CD spectra might suggest the alternation of the molecular stacking and the structure change of the supramolecular assembly induced by the photoisomerization of the **A** units. Indeed, as observed by TEM (Figure S7), morphology of the supercoil changes in response to the light irradiation. Irradiation with UV light for 20 mins results in damage of the helical structure. The screw thread became vague and holes appeared on the fibers. While illuminated with 420 nm for more than 30 mins, the morphology of the aggregates cannot recover, indicating the irreversible assembling in short term. If irradiate the aggregates in the solid state on the copper grids, almost no morphological change was observed. It might be due to the strong interaction between the aggregates and the copper grids, which restrict either the isomerization of the **A** units, and the structure transformation of the aggregates. In brief, the azobenzene units within the supercoils are light-responsible, and macroscopic effects can be triggered by photo-induced alternation of the dipole moment and geometry at the molecular level, resulting in transformation from the ordered supramolecular structure to less ordered molecularly stacking state. The structure change and application of the photoresponsible supramolecular assembly will be studied in detail in our future work.

Conductivity of the supercoils

Highly proton conductive materials are promising fuel cell that can convert chemical energy into electrical power. It was demonstrated that protons, which are available for transfer, can be readily created from highly ordered self-assembling organic molecules through hydrogen bonds and other interactions,[27,28] while proton-conducting of the assembly systems remains far from being explored. Recently, a highly conductive material for protons based on a crystalline nano-assembly of trimesic acid and melamine (TMA•M) has been reported.[28] In view of the structure of the obtained supercoil, high conductivity for proton is expected. The conductivity characterization of the supercoils was explored based on direct current–voltage (*I–V*) measurement with a two-electrode device. Appropriate amounts of supercoils were deposited by drop-casting on a silicon wafer, where the Au electrodes were thermally evaporated by mask method. The conductivity was measured in anhydrous and humid environments at ambient temperature, respectively, and the obtained *I–V* characteristics are shown in Figure 5. It is well characterized that the *I–V* curve obtained at a relative humidity (RH) of 100 % demonstrated a typical electrolyte conductive property with linear curve (Figure 5a), while that measured in anhydrous is a semiconductive property (Figure 5b). The maximum conductivity in 100 % RH is 0.13 S cm^{-1}. The conductivity increases 10^6 times when the RH increases from anhydrous to 100 %. These results suggest that in anhydrous environment, the conductivity originates from electron transportation; while in high RH environment, the high conductance should be deduced from the proton conduction between the **A** and **M** components, where proton transfer was clearly proved by the ^{1}H NMR (vid. Supra, Figure S4). It is claimed that as for a proton-conductive material, other than the protons to conduct, another requirement is necessary: a means to transport the proton.[28] According to Grotthuss mechanism,[28-30] highly ordered water chains residing in the pores of the 1D crystal structure can efficiently transfer the numerous available protons through the formation of H-bonds with excess protons. For intensive study of the proton transfer between **A** and **M**, crystal of the **M** and benzoic acid (**BA**) counterpart was obtained from the same conditions as those formed for the **M•A$_3$** supercoils. Instead of the supramolecular aggregations, crystals with 1D rod-like structure are obtained with sufficient quality for X-ray diffraction. As clearly indicated (Figure S8), **M** and **BA** interconnected through H-bonding in 2:3 ratio within the crystal. It is noted that, all the protons on the **BA** are transferred onto the N atom of the triazine, resulting in identical –C–O bonds of the benzoic acid units. Thus, each **BA** molecule provides one free proton as the origin of the proton conduction. Besides, water molecules are associated with **M** and **BA** respectively, through H-bonding to form highly ordered water channels, which is parallel to the direction of the crystal rods and responsible for transferring the numerous available protons of the acid–base complex.[28] Similar chemistry related to proton conduction is proposed for the present supercoils based on the **M•A$_3$** components, where highly ordered structure is presented and the water channel is inevitably there according to the TGA analysis (Figure S3). Therefore, the excellent conductive property of the supercoils is highly relies on the ordered stacking of the hydrogen-bonded **A** and **M** pairs, where proton transfer proceeds through water channels by a Grotthuss mechanism.

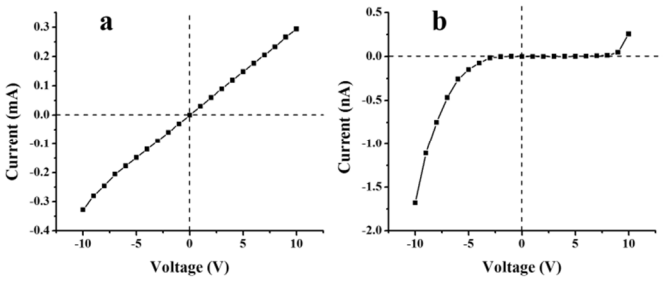

Figure 5. *I–V* curves of the film of the **M•A$_3$** supercoils measured at (a) a relative humidity of 100 %, and (b) in anhydrous environment at ambient temperature.

Conclusions

In conclusion, we demonstrate that achiral molecular components can self-organized into micron-sized supercoils, which is critical for understanding of the self-assembly processes, symmetry breaking, and amplification of the chirality. Hierarchical assembly is presented, where a pair of achiral triply H-bonded complementary components, **A** and **M** associate into **M•A$_3$** complex with C_3 symmetry, inducing a 1D helical stack by the π-interactions in synergy with the H-bonding. A kinetically controlled secondary nucleation takes place in which the one-dimensional helixes bundle into a higher ordered supercoil structure that is optically active. The supercoils demonstrate high proton-conductive property in humid environment, which is relying on the proton transfer between **A** and **M** within the highly ordered structure. The present findings provide a rational approach to the hierarchical organization of complex nanostructures and they open up new possibilities for the design of integrated molecular components in smart optical and electronic nanodevices.

Acknowledgements
The financial supports from National Natural Scientific Foundation of China (NNSFC) project (21001068) and (21371109) are gratefully acknowledged. We also thank for the financial support from the "Taishan Scholar" project of Shandong Province.

Notes and references
[a] Key Laboratory for Colloid & Interface Chemistry, Shandong University, Education Ministry, Jinan, 250100, P. R. China
[b] Key Laboratory of Functional Crystal Materials and Device, Shandong University, Ministry of Education, Jinan, 250100, P. R. China

Electronic Supplementary Information (ESI) available: [Fluorescence spectra, IR data, thermal gravimetric analysis, elemental analysis, ^{1}H NMR analysis, Wide-angle X-ray diffraction, UV-vis spectra and TEM image as well as crystal structure data]. See DOI: 10.1039/b000000x/

1. M. A. Mateos-Timoneda, M. Crego-Calama, and D. N. Reinhoudt, *Chem. Soc. Rev.*, 2004, **33**, 363–372.
2. S. Toshimi, M. Mitsutoshi, and M. Hiroyuki, *Chem. Rev*., 2005, **105**, 1401−1443.
3. M. Q. Zhao, Q. Zhang, G. L. Tian, and F. Wei, *Nanoscale*, 2014, DOI: 10.1039/c4nr00271g
4. (a) S. Cantekin, H. M. M. ten Eikelder, A. J. Markvoort, M. A. J. Veld, P. A. Korevaar, M. M. Green, A. R. A. Palmans, and E. W. Meijer, *Angew. Chem*. 2012, **124**, 6532–6537; *Angew. Chem. Int. Ed.*, 2012, **51**, 6426–6431; (b) P. J. M. Stals, P. A. Korevaar, M. A. J. Gillissen, T. F. A. de Greef, C. F. C. Fitié, R. P. Sijbesma, A. R. A. Palmans, and E. W. Meijer, *Angew. Chem. Int. Ed*., 2012, **51**, 11297−11301.
5. (a) J. Yuan, and M. H. Liu, *J. Am. Chem. Soc*., 2003, **125**, 5051–5056; (b) X. Huang, and M. H. Liu, *Chem. Commun*., 2003, 66–67; (c) X. Huang, C. Li, S. G. Jiang, X. S. Wang, B. W. Zhang, and M. H. Liu, *J. Am. Chem. Soc.*, 2004, **126**, 1322–1323; (d) P. Z. Guo, L. Zhang, and M. H. Liu, *Adv. Mater.*, 2006, **18**, 177–180; (e) Y. F. Qiu, P. L. Chen, P. Z. Guo, Y. G. Li, and M. H. Liu, *Adv. Mater.*, 2008, **20**, 2908–2913.
6. (a) Q. C. Hu, Y. Y. Wang, J. Jia, C. S. Wang, L. Feng, R. H. Dong, X. Sun, and J. C. Hao, *Soft Matter*, 2012, **8**, 11492–11498; (b) L. L.Ma, J. Jia, T. Yang, G. Z. Yin, Y. Liu, X. Sun, X. T. Tao, *RSC Adv*.**,** 2012, **2**, 2902–2908.
7. K. Mutsumi, H. Tatsuya, N. Hirotaka, T. Junko, F. Tadashi, T. Yoko and S. Hirofusa, *Chem. Mater.*, 2010, **22**, 5732–5738.
8. (a) C. Seda, F. A. G. Tom, and R. A. P. Anja, *Chem. Soc. Rev.*, **2012**, *41*, 6125−6137; (b) M. Peterca, M. R. Imam, C. H. Ahn, V. S. K. Balagurusamy, D. A. Wilson, B. M. Rosen, and V. Percec, *J. Am. Chem. Soc.*, 2011, **133**, 2311–2328.
9. (a) J. Xu, G. L. Wu, Z. Q. Wang, and X. Zhang, *Chem. Sci*., 2012, **3**, 3227−3230.; (b) K. Liu, Y. T. Kang, Z. Q. Wang, and X. Zhang, *Adv. Mater.*, 2013, **25**, 5530–5548; and the references therein.
10. B. Roy, P. Bairi, and A. K. Nandi, *RSC Adv.*, 2014, **4**, 1708–1734.
11. (a) A. Saha, S. Manna and A. K. Nandi, *Chem. Commun.*, 2008, 3732–3734; (b) P. Bairi, B. Roy, and A. K. Nandi, *J. Phys. Chem. B* 2010,**114**,11454–1146.
12. (a) J. Barberá, L. Puig, P. Romero, J. L. Serrano, and T. Sierra, *J. Am. Chem. Soc.*, 2006, **128**, 4487–4492; (b) F. Vera, R. M. Tejedor, P. Romero, J. Barberá, M. B. Ros, J. L. Serrano, and T. Sierra, *Angew. Chem., Int. Ed*., 2007, **46**, 1873–1877; (c) A. A. Vieira, H. Gallardo, J. Barbera, P. Romero, J. L. Serrano, and T. Sierra, *J. Mater. Chem.*, **2011**, *21*, 5916–5922; (d) F. Vera, J. Barberá, P. Romero, J. L. Serrano, M. B. Ros, and T. Sierra, *Angew. Chem. Int. Ed*., 2010, **49**, 4910–4914; (e) F. Vera, J. L. Serrano, M. P. D. R. Santo, M. B. Barberi, and R. T. Sierra, *J. Mater. Chem.*, 2012, **22**, 18025–18032.
13. D. L. Wang, Y. J. Huang, J. J. Li, L. Xu, M. M. Chen, J. J. Tao, and L. B. Li, *Chem. Eur. J.*, 2013, **19**, 685–690.
14. J. F. Xu, Y. Z. Chen, D. Y. Wu, L. Z. Wu, C. H. Tung, and Q. Z. Yang, *Angew. Chem. Int. Ed*., 2013, **52**, 9738–9742.
15. B. -C. Yu, Y. Shirai, and J. M. Tour, *Tetrahedron*, 2006, **62**, 10303–10310.
16. (a) Y. Chen, M. Bouvet, T. Sizun, Y. Gao, C. Plassard, E. Lesniewska, and J. Jiang, *Phys. Chem. Chem. Phys*., 2010, **12**, 12851–12861; (b) J. Kan, Y. Chen, J. Gao, L. Wan, T. Lei, P. Ma, and J. Jiang, *J. Mater. Chem.*, 2012, **22**, 15695–15701.
17. T. Fujii, H. Kashida, and H. Asanuma, *Chem. Eur. J.*, 2009, **15**, 10092–10102.
18. A. Painelli, F. Terenziani, L. Angiolini, T. Benelli, and L. Giorgini, *Chem. Eur. J.*, 2005, **11**, 6053 – 6063.
19. D. P. Yan, G. R. Williams, M. Zhao, C. M. Li, G. L. Fan, and H. M. Yang, *Langmuir*, 2013, **29**, 15673–15681.
20. G. Zimmerman, L.Y. Chow, and U.J. Paik, *J. Am. Chem. Soc.*, 1958, **80**, 3528–3531.
21. T. Schultz, J. Quenneville, B. Levine, A. Toniolo, T. J. Martínez, S. Lochbrunner, M. Schmitt, J. P. Shaffer, M. Z. Zgierski, and A. Stolow, *J. Am. Chem. Soc.*, 2003, **125**, 8098–8099.
22. A. Cembran, F. Bernardi, M. Garavelli, L. Gagliardi, and G. Orlandi, *J. Am. Chem. Soc.*, 2004, **126**, 3234–3243.
23. (a) C. W. Chang, Y. C. Lu, T. T. Wang, and E. W. G. Diau, *J. Am. Chem. Soc.*, 2004, **126**, 10109–10118; (b) E. W. Diau, *J. Phys. Chem. A.*, 2004, **108**, 950–956.
24. T. Cusati, G. Granucci, E. Martínez-Núñez, F. Martini, M. Persico, S. Vázquez, *J. Phys. Chem. A.*, 2012, **116**, 98–110.
25. N. Tamai, H. Miyasaka, *Chem. Rev.*, 2000, 100, 1875–1890.
26. (a) M. Mathews, R. S. Zola, S. Hurley, D. Yang, T. J. White, T. J. Bunning, and Q. Li, *J. Am. Chem. Soc.* 2010, **132**, 18361–18366; (b) Y. Wang, A. Urbas, and Q. Li, *J. Am. Chem. Soc.*, 2012, **134**, 3342−3345; (c) Y. Wang, and Q. Li, *Adv. Mater.*, 2012, **24**, 1926–1945.
27. Y. B. Chen, M. Thorn, S. Christensen, C. Versek, A. Poe, R. C. Hayward, M. T. Tuominen, and S. Thayumanavan, *Nat. Chem.*, 2010, **2**, 503–508.
28. H. Wang, X. Xu, N. M. Johnson, N. K. R. Dandala, and H.-F. Ji, *Angew. Chem. Int. Ed.*, 2011, **50**, 12538–12541.
29. P. Colomban, A. Novak, *J. Mol. Struct.*, 1988, **177**, 277 – 308.
30. N. Agmon,Chem. *Phys. Lett.*, 1995, **244**, 456 – 462.

SYNOPSIS TOC

Supercoils self-assembled from achiral molecular hydrogen-bonded two-components have been studied for in-depth understanding of the structure and functionality of this chiral supramolecular association.

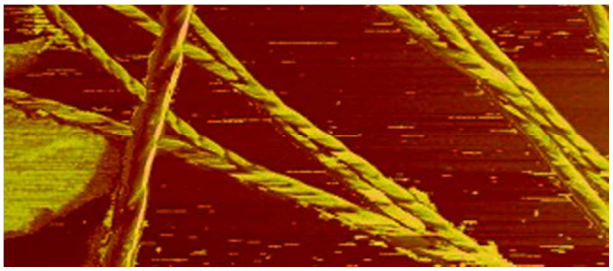

Table of Contents artwork